PFG (2021) 89:487–503
https://doi.org/10.1007/s41064-021-00162-z

ORIGINAL ARTICLE

Re-engineering the Past: Countrywide Geo-referencing of Archival Aerial Imagery

Holger Heisig[1] · **Jean-Luc Simmen**[1]

Received: 16 February 2021 / Accepted: 3 September 2021 / Published online: 22 September 2021

Abstract

Archival aerial imagery (AAI) represents a unique and relatively unexploited resource for assessing long-term environmental changes at a very high spatial resolution. A major constraint for the wider use of AAI often lies in the difficulties of establishing precise geo-referencing, namely in the difficult and time-consuming task of assigning ground reference through manual digitization of Ground control points (GCPs). We present a highly automated photogrammetric workflow for orientation of AAI. The workflow substitutes manual GCP measurements by generating image matches to a digital reference. The resulting abundant observations are algorithmically filtered and used in a bundle block adjustment (BBA) to obtain final image orientations. The proposed workflow has successfully been employed to process a complete coverage of AAI over the territory of Switzerland based on images acquired between 1985 and 1991. The accuracies obtained from the orientation process are very satisfying and allow for generating meaningful 2D and 3D products. The absolute accuracy for derived orthophotos and their mosaics is about 1 m. The relative accuracies are in the subpixel range and allow for generation of country-wide Digital surface models (DSMs) through dense-image matching. The obtained accuracies are comparable to those obtained at the authors' affiliation using classical workflows that involve manual GCP identification from digital reference data. With regard to human working time, the workflow has, in our case, proven to be at least five times more efficient than classical workflows whilst the required computational resources are very moderate.

Keywords Photogrammetry · Orientation · Co-registration · Geo-referencing · Analog · Aerial · Matching · Automation · Switzerland

Zusammenfassung

Für die Erfassung langfristiger Umweltveränderungen stellen historische Luftbilder eine einzigartige und relativ wenig genutzte Datenquelle sehr hoher räumlicher Auflösung dar. Ein Haupthindernis für eine breitere Nutzung historischer Luftbilder liegt häufig in den Schwierigkeiten der Erstellung einer präzisen Georeferenzierung. Dies betrifft insbesondere die zeitaufwändige manuelle Digitalisierung von Ground Control Points (GCPs). Wir stellen einen hochautomatisierten photogrammetrischen Workflow für die Orientierung historischer Luftbilder vor. Der Workflow ersetzt manuelle GCP-Messungen durch automatisiertes Bild-Matching mit einer digitalen Referenz. Die daraus resultierenden zahlreichen GCP-Beobachtungen werden algorithmisch gefiltert und zusammen mit automatisch generierten Verknüpfungspunkten in einer Bündelblockausgleichung (BBA) gerechnet, um die endgültige Bildorientierung zu erhalten. Der vorgeschlagene Workflow wurde erfolgreich eingesetzt, um eine vollständige Abdeckung historischer Luftbilder über dem Gebiet der Schweiz aus Luftbildern aus den Jahren 1985 bis 1991 zu erstellen. Die durch den Orientierungsprozess erzielten Genauigkeiten sind sehr zufriedenstellend und ermöglichen die Erstellung aussagekräftiger 2D- und 3D-Produkte. Die absolute Genauigkeit der abgeleiteten Orthophotos und ihrer Mosaike liegt bei etwa 1 m. Die relativen Genauigkeiten liegen im Subpixelbereich und ermöglichen die Erstellung landesweiter digitaler Oberflächenmodelle (DOMe) durch Dense-Image-Matching. Die erzielten Genauigkeiten sind mit denen vergleichbar, die in der Organisation der Autoren mit klassischen Arbeitsabläufen erzielt wurden, welche eine

✉ Holger Heisig
holger.heisig@swisstopo.ch

[1] Federal Office for Topography swisstopo, Seftigenstrasse 264, CH-3084 Wabern, Switzerland

manuelle GCP-Identifizierung aus digitalen Referenzdaten beinhalten. In Bezug auf die menschliche Arbeitszeit hat sich der vorgestellte Workflow in unserem Fall als mindestens fünfmal effizienter als klassische Workflows erwiesen, während die erforderlichen Rechenressourcen sehr moderat sind.

1 Introduction

Aerial photos can literally be seen as one of the most important immediate visual testimonies of the Earth's surface. Aerial imagery with country-wide coverage has systematically been acquired since the 1930s by National Mapping and Cadastral Agencies (NMCAs) or military cartographic sections (Redweik et al. 2010). Today, a time series of archival aerial imagery (AAI) can reveal a huge yet vastly unexploited potential for retrospectively assessing long-term environmental changes (Pinto et al. 2019; Giordano et al. 2018). A rapidly growing interest in the use of historical aerial photos and their derivatives was observed over recent years. The interest comes from domains of application as diverse as archaeology (Verhoeven et al. 2013; Cowley and Stichelbaut 2012), forest sciences (Bożek et al. 2019; Nurminen et al. 2015), historic landscape and settlement analysis (Nebiker et al. 2014; Mertes et al. 2017; Sevara et al. 2018; Gomez et al. 2015), glaciology(Mölg and Bolch 2017) (Vargo et al. 2017) (Fischer et al. 2011) or geomorphology (Micheletti et al. 2015; Ford 2013; Strozzi et al. 2013). Due to recent developments in dense-image matching (Remondino et al. 2014), special interest is often given to the multi-temporal analysis of Digital Elevation Models (DEMs) derived from historical aerial photos.

The challenges in fully exploiting the potential of AAI for environmental studies include their exposure to physical and chemical deterioration, the multitude of applied acquisition systems, missing or incomplete metadata, the heterogeneous radiometric properties of corresponding image scans and the problems encountered in establishing precise geo-referencing (Giordano et al. 2018).

Precise geo-referencing is a mandatory pre-requisite for relating aerial images to other geodata, e.g. by use of Geographic Information Systems (GIS). Photogrammetric approaches are the most established means to perform geo-referencing of aerial images. These approaches aim at modelling the internal and external orientation elements of a number of overlapping images defined as an aerial triangulation (AT) block. Classical photogrammetric workflows for orientation of AAI typically encompass the following steps:

1. Measurement of fiducial marks: provided sufficient image scan quality is available, the detection of fiducial marks in the image scan files can be carried out in fully automated mode.
2. Measurement of tie points (TP): tie points identify common features on overlapping images. Detection and matching of TPs is nowadays typically carried out in a fully automated mode (Bożek et al. 2019; Bakker and Lane 2017; Feurer and Vinatier 2018; Fischer et al. 2015).
3. Measurement of ground control points (GCPs): coordinates from a reference are assigned to manually identified points in the images. The reference coordinates may either come from field measurements (Strozzi et al. 2013) or are extracted from digital reference data like road vector data or orthophotos (Mertes et al. 2017; Mölg and Bolch 2017). The task of manual GCP digitization in AAI is often referred as being difficult, error-prone and time consuming. Most authors explicitly mention the difficulty of identifying well-defined points that are stable over time in both, reference and historic aerial photo.
4. Bundle block adjustment (BBA): the modelling of accurate viewing geometries is commonly achieved through bundle block adjustment. In bundle block adjustment, which is based on the collinearity equations, the TP and GCP observations together with the cameras' interior orientations are used to estimate the unknowns: the elements of exterior orientation and the 3D coordinates of the tie points. In this way, photogrammetric approaches "re-engineer" the original pose of the camera at acquisition time.

Once established, precise orientation elements allow for (1) extraction of 3D geo-information by visual stereoscopic interpretation, (2) automated extraction of Digital Surface Models (DSMs) and (3) production of orthophotos and orthomosaics.

Like other NMCAs, the Swiss Federal Office of Topography swisstopo holds a large collection of historic aerial imagery. The systematic acquisition of aerial photographs in Switzerland began in 1926. National aerial photography campaigns, organised in constant cycles, allowed for continuous updates of the national topographic maps. swisstopo's archive image collection contains about 400,000 aerial photographs. Only a small portion of these photos have so far been oriented. Important country-wide uses of swisstopo's oriented archival aerial images have been established, though. This concerns stereoscopic visual analysis for assessing land use statistics (Beyeler 2010), historical DSM generation (Ginzler and Hobi 2015; Ginzler et al. 2019) and orthomosaic generation (swisstopo 2021a). Growing physical and chemical deterioration of the image collection has led to extensive conservation and digitization measures from

2010 onwards. The measures on swisstopo's aerial image collection include: conservation measures on the originals, long-term storage of originals in climatized rooms, photogrammetric scanning of originals, metadata collection and its management. Customers can purchase digital copies of all scanned archival aerial imagery. Alternatively, full resolution image files, together with basic metadata, can freely be consulted through a web service (swisstopo 2021b).

For ease of public access to the image information, precise geo-referencing of all scanned aerial images as well as production and publication of orthomosaics is highly desirable. Figure 1 displays the general workflow from the original analogue images to orthomosaics. Due to limited resources for establishing precise geo-referencing in a classical photogrammetric workflow, a need for a highly automated photogrammetric workflow capable of efficiently orienting thousands of aerial photos with high accuracy was identified at swisstopo.

In classical photogrammetric workflows, the establishment of exterior image orientation was identified as being the most time-consuming step in the image orientation process. Despite early attempts (Heipke 1997), surprisingly few methods have been proposed to overcome this issue (Giordano et al. 2018):

Minimization of the number of GCPs by geostatistical methods has been proposed by Persia et al. (2020). Co-registration on the basis of stable linear features is presented by Nagarajan and Schenk (2016); Cléry et al. 2014). Manual digitization of these linear features in archival imagery and ground reference are still required in Nagarajan and Schenk (2016). Cléry et al. (2014) proposes matching of extracted lines in archival images to a vector reference of linear features. A method for automatic detection of GCPs was presented by Giordano et al. (2018). The GCPs are detected in recent orthophotos and then transferred to archival imagery. The method relies on the detection of keypoints between images of different times.

Despite the encouraging results reported from the different authors, none of the proposed methods was reported to be implemented on a production scale.

Note that the use of the notion Ground *Control* Points in the context of automated collection is not unproblematic, since the points are not (user-) *controlled*. As these reference points fulfil the same function in BBA as user controlled points, we will stick to the notion of *GCPs* for automatically collected points in this article.

In this study, we applied an extended workflow based on the commercial software package HAP (*Historical Air Photo*) from the software provider *PCI Geomatics* to process a country-wide coverage of aerial images taken between 1985 and 1991.

The main objectives of the present study are: (1) to demonstrate the highly automated workflow to achieve precise geo-referencing of a national coverage of AAI; (2) to evaluate accuracies obtained for the orientations and derived products; (3) to estimate the overall efficiency of the proposed workflow and (4) to present the potential and limitations of the workflow by discussing its transferability into time and space.

2 Materials and Methods

2.1 Study Area

The study area comprises the entire Swiss territory that covers 41,285 km^2. The Swiss Alps constitute about 60% of the country's total area. According to federal land use statistics from 2013 (Swiss Federal Statistical Office 2021), the predominant types of land use in Switzerland are agriculture and farming (36.9%) forests and woodlands (30.8%) and unproductive areas (25.5%). Unproductive areas comprise lakes, rocks, glaciers and perpetual snow. Settlements account for 6.8% of the national territory. With its high variation in altitude (200–4600 m a.s.l.) and its big variety of land use and cover, the study region represents a most challenging test ground for a highly automated photogrammetric workflow.

Orientation and product creation in this study is carried out in the reference system of the Swiss national survey 1903 (EPSG:21781). The reference system bases on the Mercator projection and the Bessel ellipsoid. The vertical reference system is the Swiss height reference system LN02 (swisstopo 2021c).

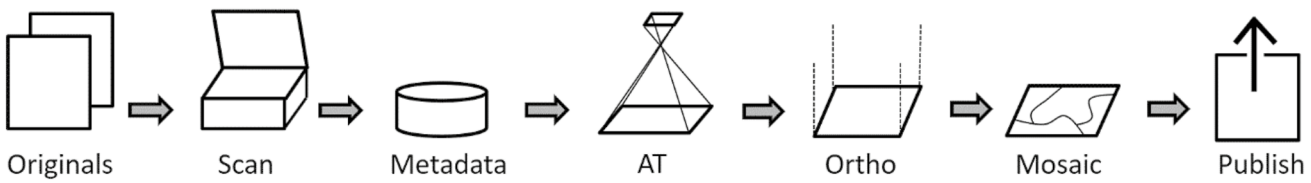

Fig. 1 General workflow from aerial image originals to published digital orthomosaics. (*AT* = aerial triangulation)

2.2 Data

2.2.1 Aerial Image Data

The aerial images processed in the scope of this article were captured by swisstopo between 1985 and 1991. The set consists of 8′507 aerial images covering the complete Swiss territory in full stereo mode. According to flight reports, the average image scale is around 1:25′600, the minimum image scale is around 1:35′300. The annual acquisition zone was divided into an alpine sub region and a sub region in the lowlands. The images of the lowland regions were acquired under snow-free and cloud-free conditions with leaves off during springtime (March to June). The images of the alpine regions were acquired between July and September to assure equally snow-free images. The regions of Zürich and Geneva were covered twice in the given period. The flying height varied in function of topography between 4000 and 7000 m a.s.l. The overlap in-flight direction varies, again depending on the topography, between 60 and 80%. The lateral overlap is about 20–25%.

In general, all flight lines are oriented East–West or vice versa. Exceptions to this rule occur in larger alpine valleys where supplementary flight lines were flown at lower altitudes. The azimuthal orientation of these valley lines follows the topography of the valley. Figure 2 gives an overview of flight line geometries.

All images of this data set were digitised at swisstopo during the past years using the Leica DSW 700 photogrammetric scanner. The original image negatives were scanned with a geometric resolution of 14 µm per pixel and a radiometric resolution of 8 bit. The average ground sampling distance (GSD) resulting from image scale and scan resolution is 35 cm, the maximum GSD is 49 cm.

2.2.2 Aerial Image Metadata

With the conservation and digitization measures taken in recent years, a complete set of metadata was collected. Primary sources of metadata included information from flight plans, flight reports, calibration protocols, etc. The collected metadata are managed in an Aerial Image Information System (*Luftbildinformationssystem LUBIS*). The LUBIS metadata system consists of a geo-relational DBMS running on ArcSDE/Oracle.

Initial geo-referencing for the archived images is obtained as follows: the first and the last image of each flight line is manually located in X and Y in the 3D coordinate space. The accuracy for these values is estimated to be 100–300 m. The flying height is derived from flight report. All image

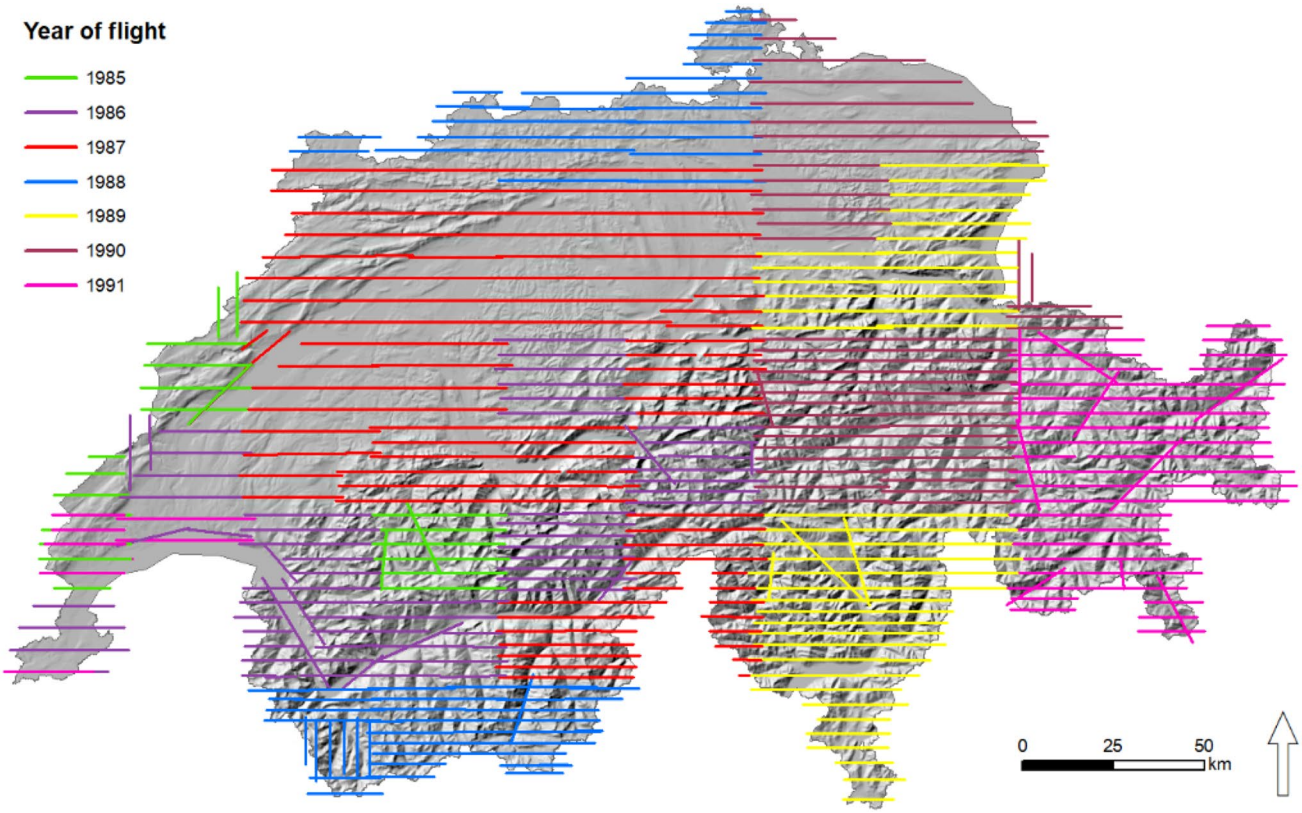

Fig. 2 Geometry and flight year of flight lines. Initial geo-referencing results in straight lines

projection centres belonging to the same flight line are derived through interpolation following the order of image acquisition. Each flight line's projection centres thus lie on a straight line. The accuracy of the interpolated projection centres varies depending on the length of the flight line and the corresponding flight conditions (e.g. accuracy of navigation, wind) between 100 m and around 4000 m.

A camera of the type Wild RC10 with a Leica 15/4 UAG lens was used for the acquisition campaigns processed in this study. The image format is 23 cm * 23 cm. The calibration protocol that was assumed valid for the entire acquisition cycle has been digitised into the LUBIS system. The calibrated focal length is given with 153.37 mm.

The 8′507 images to be processed were grouped into 36 blocks for aerial triangulation. The repartition is displayed in Fig. 3. For each image, a block identifier was added to LUBIS. Blocks were primarily defined by spatial coherence. Temporal coherence was a criterion to be neglected due to the short time span (6 years) of image acquisition. The size of the blocks varied between 70 and 700 images.

2.2.3 Reference and Auxiliary Data

The external orientation in our proposed workflow is determined by the use of GCPs that are automatically collected from reference data sets. The planimetric reference coordinates of the GCPs are derived from an orthoreference, the height information from a DEM.

Our orthoreference is the Swiss national orthomosaic SWISSIMAGE (swisstopo swissimage 2021). The reference year of the utilised orthomosaic version is 2016. The SWISSIMAGE product consists of a complete and cloud-free coverage of seamlessly mosaicked orthorectified aerial images acquired between 2014 and 2016. The absolute planimetric accuracy of these data is defined with a standard deviation of 25 cm. The original RGB product with a pixel size of 25 cm has been resampled to 3 m for the coarse alignment run and to 1 m for the fine alignment run. The resampling is carried out to account for the geometric resolution of the corresponding image pyramid layers used in the alignment process. As we matched panchromatic images only, a panchromatic derivative from SWISSIMAGE was produced.

The national orthophoto mosaic SWISSIMAGE is furtherly used in its full resolution to measure the accuracy of the obtained orthorectified image products.

For assigning height information to GCPs we used the Swiss national height model product swissALTI3D (swisstopo swissALTI3D 2021) from the reference year 2016. This Lidar-based Digital Terrain Model (DTM) with country-wide coverage has a vertical accuracy with a defined

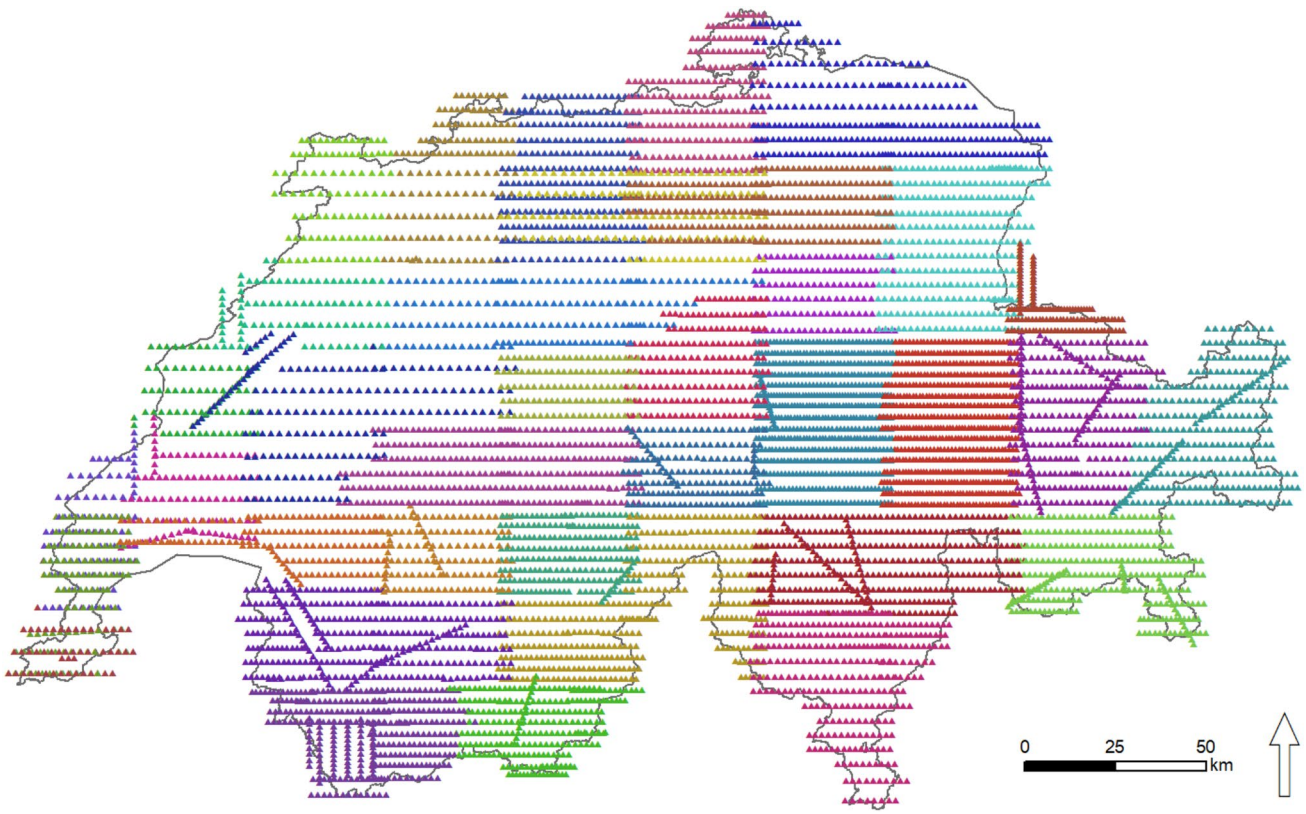

Fig. 3 Repartition of aerial images into 36 contiguous blocks

standard deviation of 50 cm. The utilised height model has 2 m pixel size. The height model is also used in the later orthorectification process.

For the GCP collection process, the derived orthoreference has been masked by *NoData* values for land cover classes which are highly likely to produce erroneous matches. These land cover classes comprise water surfaces, glacier surfaces and forested surfaces. Data from the Swiss Topographic Landscape Model (swissTLM3D) (swisstopo swissTLM3D 2021) were used to define the masks.

2.3 Orientation of Image Data

2.3.1 The HAP Core Process

The developed workflow is based on the commercial software package *HAP* (Historical Air Photo) from the remote sensing software provider *PCI Geomatics*. HAP itself uses the functionality defined within PCI's photogrammetric software product *OrthoEngine*. The orientation process was performed with version 2018 SP1. The HAP bases on the functionality of a fully featured photogrammetric workflow. Its components can either be executed through a graphical user interface (GUI) or, with advanced capabilities, by calling associated Python routines through scripting applications. Apart from a White Paper (Melamed 2013), no public technical documentations about HAP are available. Therefore, its core functionality needs to be briefly summarised here. The traceability of the process is given through the Python scripts through which HAP is executed. Figure 4a summarises the workflow recommended by the software provider. It consists of following steps:

1. Data preparation process: in the data preparation, a metadata file in text format is manually prepared. The file contains metadata for each image of the aerial triangulation block. Required metadata include the image file name, its approximate exterior orientation (projective centre coordinates in X, Y and Z), the image size and the focal length of the camera.
2. Ingest process: the so-called ingest process creates an ASCII-based photogrammetric project file based on the metadata text file. The process imports the image scan files into PCI's intrinsic PIX format and links them to the project file. The project file is stepwise updated during the further processes. Internally, the orientation angles omega and phi angles are set to zero in the initial state, whereas the kappa corresponds to the azimuth of the flight line.
3. Interior orientation: after running the ingest process, automated fiducial mark detection is carried out in order to establish the interior orientations of the images. For a given project, the user is required to digitise fiducials on a template image. A routine is then launched to detect fiducials automatically in all other images belonging to the same project. Details about the utilised algorithm are not available in the software documentation.
4. Alignment process: the following (so-called) alignment process automatically identifies GCPs and TPs and filters these to user-defined error thresholds. The process requires as input the photogrammetric project file, the reference orthophoto file and the DEM file. Parameters for the collection of points, e.g. intended point density, search radius, the image pyramid level, the point matching method and the minimum correlation score, can either be provided through the GUI or in a parameter file. The GCP Collection is conducted using phase matching, which identifies corresponding keypoints between images in the frequency domain. Further details about the utilised algorithm are not available in the software documentation. GCP collection and filtering is carried out independently for each image. Therefore, no stereo measurements of GCPs are established. After successful GCP candidate detection, a RANSAC based algorithm (Fischler and Bolles 1981) is employed for removal of outliers. Once the GCP collection is completed, the TP collection and filtering process are run. Based on image footprints from the initial geo-referencing and the search radius, image tuples are identified for the TP collection. After completing the TP detection, the

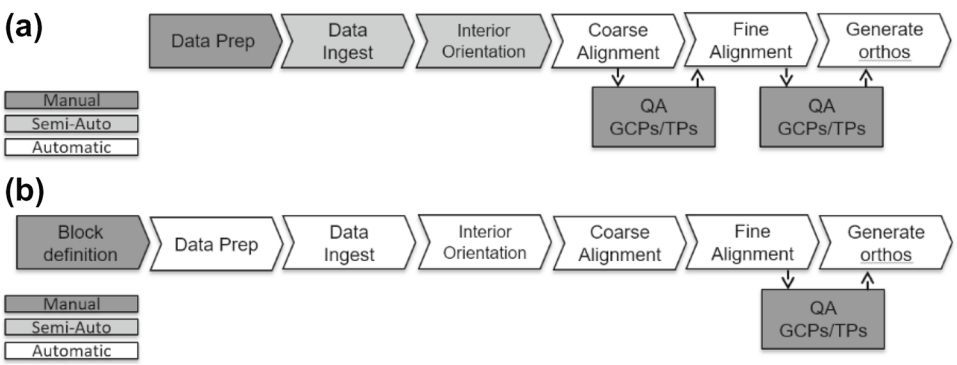

Fig. 4 Schematic of the HAP workflow. **a** Original workflow; **b** our adapted workflow

automatic TP refinement is carried out. The refinement step identifies TPs with higher residuals after running BBA. These TPs are then removed from subsequent processing. The TP refinement step is implemented as an iterative process. The result of the alignment process is a potentially large number of collected and filtered GCPs and TPs that are saved to the photogrammetric project file. The HAP software uses a multi-resolution matching approach for both TP and GCP collection. In our case, the TP collection was, e.g. parametrized to use the 8 * 8 pyramids and the full resolution images, GCP collection should be parametrized to end on a pyramid level which corresponds best to the GSD of the reference orthophoto file. Details about the utilised algorithm for GCP and TP detection are not available within the software documentation.

5. Quality Assurance (QA): this step corresponds to the validation and improvement of the results of the automated processing in an interactive process. First, good connectivity of all images of the block should be assured. In case of missing measurements, GCPs/TPs may need to be added by either manual digitization or by re-running automated GCP/TP collection locally from within the OrthoEngine project. Persisting blunders are identified and eliminated in an iterative procedure of evaluating BBA results, performing edits to TPs and GCPs and re-running BBA again. The aim of the QA process following the first alignment process is a substantial improvement of exterior orientation (EO) parameters compared to the initial geo-referencing.

The software provider recommends executing alignment runs and interactive QA steps in an iterative procedure. Improved image orientations after the first QA step serve as input to the next alignment run. In this second run, parameters adapted to the improved EO can be used. In a second alignment run, e.g. the search radius or the image pyramid level may be lowered to account for the improvement of EO. Therefore, the first alignment run is referred to as *coarse alignment* whereas consecutive alignment runs are referred to as *fine alignment*. The orientation process ends when the user is satisfied with the results from his/her last QA step.

In summary, the HAP system can be described as a highly automated photogrammetric workflow tailored for bulk orientation of AAI. One of its principal advantages consists of relieving the user from the potentially time-consuming step of manual GCP detection. HAP is tailored for processing imagery with sparse metadata.

Limitations in the performance of the system or to the quality of the output may, for example, originate from insufficient image or scan quality, cloud cover, insufficient quality of reference files, or initial geo-referencing being too imprecise.

2.3.2 Workflow Adaptation and Process Parametrization

Following a close examination of the original HAP workflow, it was found that the workflow proposed by the software provider exhibited further potential for automation. The following adaptations to the workflow have been implemented:

1. Automated data preparation: a data preparation routine has been developed and implemented into the *Feature Manipulation Engine* (FME) software. The routine prepares all required image data, metadata and reference data for the HAP processing on a per-block base. The reference orthophoto and DEM files are clipped to the buffered geographic extent of footprints from initial geo-referencing of the current aerial triangulation block. Land cover classes not suited for GCP detection (water surfaces, forests, glaciers) are masked out from the reference orthophoto. The OrthoEngine Python API is employed to automatically import precise calibration information and setting the project file projection system to the Swiss national reference system.
2. Interior orientation: fiducial mark detection is carried out on a sample template image located physically in a (so-called) chip database. This omits the process of having to interactively digitise fiducials on a per-project base.
3. Omitting QA step after the first alignment and archival of orientation elements: it was found that the first alignment process improves the image orientations sufficiently well so that its output can directly be used as input to the second alignment step without any interactive QA work. Thus, the final QA step is the only manual step in the processing chain. Its importance is high, though, as it defines the final accuracy of the orientations. After acceptance of the results of BBA in the final QA process, the resulting internal and external orientation parameters are written to the meta-database LUBIS using an application developed in-house.

Our adapted workflow applied in this study thus automates the image orientation process starting after block definition in LUBIS to the final (and only) manual QA step into one single fully automated computational process. The processing of each of the 36 aerial triangulation blocks was controlled through a single batch file. From this file, the corresponding Python scripts for data preparation and HAP processing are called and executed. The complete HAP parameter definition that was utilised is given and partially discussed in Heisig (2020).

Figure 4b summarises the adapted workflow.

The processing was run on a standard PC in a Virtual Desktop Environment. The PC configuration was as follows:

Intel(R) Xeon(R) CPU E5-2667 v4 @ 2*3.20 GHz processors, 24 GB installed memory (RAM). Either three or four AT projects where run in parallel.

2.4 Generation of Image Products and Accuracy Assessment

2.4.1 Orthophoto Generation and Mosaicking

The retrieved orientation parameters allow for straightforward generation of the principal image products. Hence, orthophotos for each of the 8′507 input images have been calculated after completion of the orientation process.

The swissALTI3D DTM product with 2 m pixel size was used as an elevation source to calculate orthophotos with 50 cm pixel size in the Swiss national reference system (EPSG:21781). For maximum consistency, it would have been preferable to use an elevation model that represents the topography at the time of image acquisition. A historic height model with sufficient geometric resolution is not available at swisstopo. The option of producing a country-wide DSM from the oriented historic images themselves for the use in the orthorectification process was discarded due to the significant effort involved. By using the recent swissALTI3D height model, a time difference of around 35 years between acquisition of images and acquisition of elevation data is thus taken into account. In areas with substantial changes in terrain height such as, for example glaciers, this results in planimetric inaccuracies in the orthorectified images.

Since an orthoimage bulk production workflow existed already, the orthoimage calculation and mosaicking was not carried out with functionality provided by OrthoEngine. Instead, an in-house built application based on *OrthoMaster* from INPHO/TRIMBLE was used. To radiometrically harmonise and sharpen the resulting orthophotos, an in-house built PhotoShop macro was run on the orthoimages. After this, single orthophotos are written to the image archive.

From the orthophotos, homogeneous and cloud-free mosaics are produced in year-wise contiguous blocks. The software used in this process is *OrthoVista* from INPHO/TRIMBLE. An automated process generates a first mosaic version using automatic colour adaptation and seam line generation. The automated mosaic output is visually checked for remaining artefacts such as remaining cloud patches. The operator evaluates alternative orthoimages covering the detected problematic regions and edits the corresponding seam lines manually. No manual geometric corrections, e.g. for bridges, were carried out on orthoimages or mosaics.

The absolute geometric accuracy of the obtained orthomosaic has been assessed by comparison with the most current version of SWISSIMAGE. A set of around 300 sample points has been defined by overlaying a regular grid. Within a given radius around each grid point, the planimetric distance of an object identifiable in the reference and on the generated mosaic has been measured.

2.4.2 Generation of DSMs

DSMs can be derived from overlapping and accurately oriented aerial imagery through highly automated processing routines based on dense-image matching algorithms. In our case, no systematic DSM extraction over the whole study area was carried out due to limited resources. To demonstrate the potential, though, we generated DSMs over a number of 10 arbitrary test areas of 6 km by 9 km. The samples cover a wide range of diverse landscapes and associated land cover types in Switzerland. Masking out vegetation and buildings, the subsequent subtraction of the correlated DSM from a reference DEM allows for straightforward quantification of topographic changes such as changes in glacier volume. Using the orientation parameters stored in a database, complete DSM extraction may still be performed at a later time.

In our case, the OrthoEngine DEM extraction module has been used to calculate DEMs directly from the OrthoEngine project file. The module uses a semi-global matching (SGM)-based algorithm (Hirschmuller 2007). The extraction has been run on the images at full resolution.

3 Results

3.1 Results of the Automated Processing Chain

For all the 36 aerial triangulation blocks, the automated processing chain delivered: (1) complete and reliable positions of fiducial marks for establishing the internal orientations (IO); (2) consistently high numbers and good general distribution of both GCPs and TPs; (3) high shares of multi-ray TPs, important to ensure a robust model and (4) generally high reliability of automatically detected points.

- Results of IO: the automated fiducial detection collected four corner fiducial marks on each of the 8′507 images without failing once. The mean length of the residual vectors from automated fiducial detection amounts to 0.51 pixels with a standard deviation of 0.28 pixels and a maximum value of 1.6 pixels
- Results of TP and GCP detection: an exemplary block configuration showing automatically detected TPs and GCPs is depicted in Figs. 5 and 6. The block is numbered *AT_22*. It contains 136 images and is geographically located in the *Emmental* region. The landscape of the region is characterised by meadows and pastures and range in altitude stretches from 400 to 1400 m a.s.l.

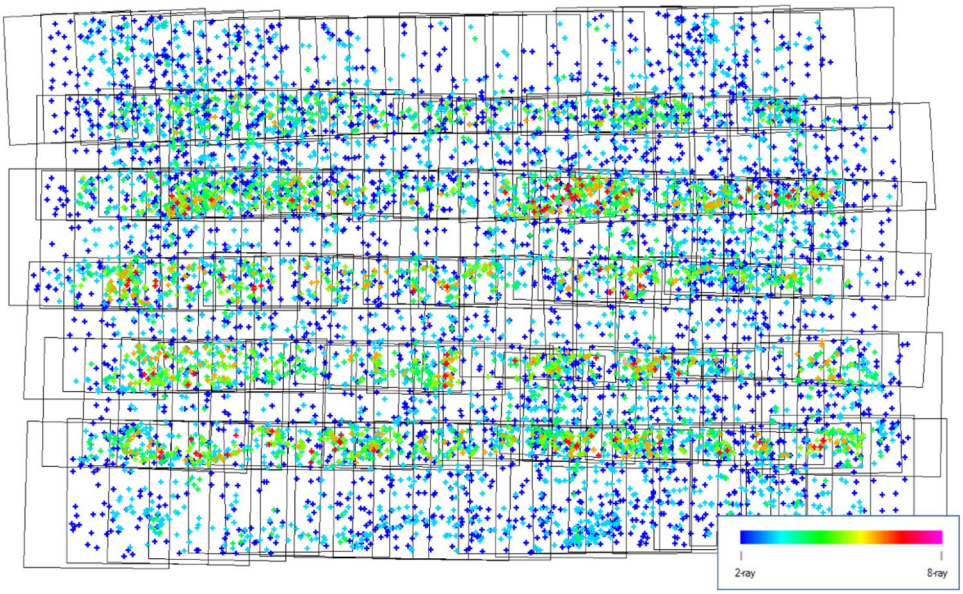

Fig. 5 Result of automated TP detection on an exemplary block. Dark blue corresponds to TPs with two rays, TPs with multiple rays are depicted in green and reddish colours

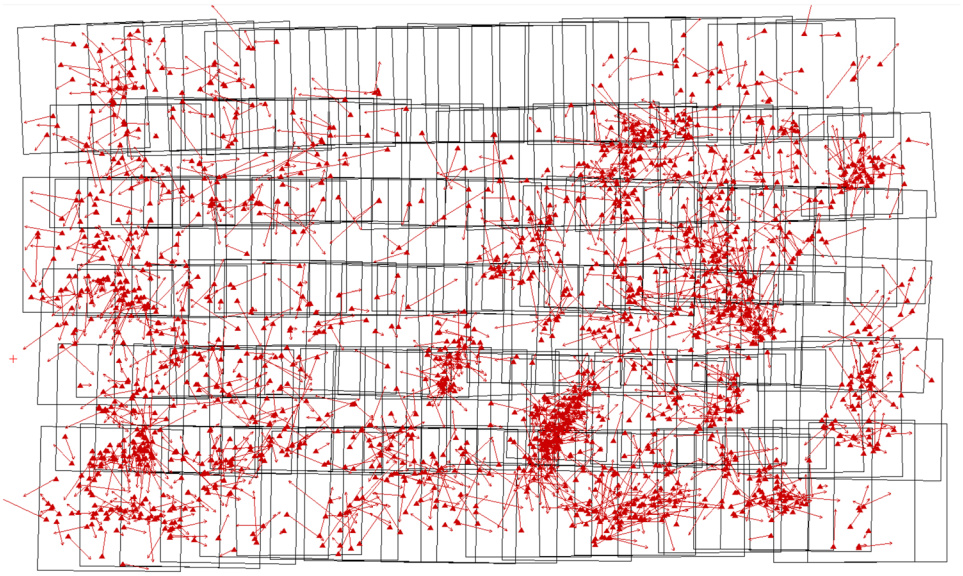

Fig. 6 Depiction of GCP distribution and residuals for the exemplary *Emmental* block. Unfortunately, OrthoEngine does not display a legend for the magnitude of GCP residuals

Table 1 summarises the number of extracted GCPs and TPs for all of the 36 AT blocks.

- Processing time: the average processing time per image was around 5–8 min, comprising all steps of the automated workflow. It is calculated by dividing the block processing time by the number of images.

3.2 Final QA

The results of the automated processing chain laid the base for conducting the final QA step in a straightforward manner for most of the defined AT projects. The final QA was carried out in two steps: (1) running BBA using TPs only; and (2) establishing exterior orientation based on the result of step 1 by running BBA with TPs and GCPs combined.

Step 1 was carried out when each image had a minimum of 4–6 well-distributed TPs and showed an RMS not much higher than one pixel. Step 2 was considered to be finished when the overall statistics from BBA showed acceptable residuals on well-distributed GCPs. The a priori accuracies for GCP coordinates during BBA were defined with 0.5 m in X, Y and Z. No self-calibration was used in BBA.

The most important techniques for iteratively arriving at the final orientations during QA work turned out to be: (1) manually adding TP measurements in order to ensure good block connectivity and a stable configuration of all images within the block; and (2) semi-automatic selection

Table 1 Summary of statistics of the orientation process

Block name	Number images	Auto-TPs		AutoGCPs		TPs manual	Max. Res. GCP X/Y [m]	Max. Res. GCP Z [m]	RMS GCP X/Y [m]	RMS GCP Z [m]
		Extracted	Retained	Extracted	RETAINED					
AT_01	625	74,683	73,174	20,846	18,066	69	3.44	1.73	0.76	0.39
AT_02	649	88,751	86,646	28,442	24,990	43	3.92	2.38	0.79	0.42
AT_03	126	16,439	15,947	5615	4996	33	3.25	2.05	0.86	0.45
AT_04	73	17,296	16,201	2518	1943	0	3.46	4.81	0.92	1.22
AT_05	132	35,082	32,305	4762	3382	0	4.38	2.17	0.84	0.39
AT_06	86	11,134	10,249	3151	2549	8	4.50	2.30	1.20	0.55
AT_07	252	33,177	31,248	8303	7240	1	3.69	3.90	0.71	0.97
AT_08	199	27,191	24,332	3330	2568	0	3.35	1.65	1.07	0.46
AT_09	260	35,914	34,836	10,429	5492	56	1.56	0.90	0.43	0.19
AT_10	128	22,706	20,428	5918	4647	4	2.48	1.17	0.69	0.30
AT_11	298	22,616	21,014	11,773	10,024	15	3.82	1.80	0.84	0.41
AT_12	292	28,358	26,870	9915	6450	0	3.70	1.90	0.81	0.37
AT_13	72	5212	4667	1948	1398	12	2.90	1.39	0.86	0.40
AT_14	97	6857	6486	4069	3059	11	3.70	1.60	0.82	0.37
AT_15	123	10,698	9929	4050	2997	9	1.96	1.11	0.65	0.28
AT_16	129	6932	6548	6527	4564	33	3.17	1.54	0.74	0.36
AT_17	62	4224	4062	2782	1729	11	1.51	0.68	0.57	0.25
AT_18	189	17,767	16,701	5696	4462	4	2.62	1.36	0.68	0.31
AT_19	185	16,891	15,734	3923	2879	52	2.84	3.03	0.82	0.45
AT_20	310	25,932	24,956	5425	4139	64	2.76	1.40	0.71	0.33
AT_21	210	26,980	25,629	3860	3124	7	3.61	1.85	0.68	0.36
AT_22	136	11,323	10,782	3119	2219	2	2.18	1.01	0.58	0.28
AT_23	183	13,947	13,282	5967	4915	66	2.81	1.31	0.67	0.35
AT_24	392	42,207	40,685	16,699	14,969	43	3.76	2.19	0.77	0.44
AT_25	231	12,691	12,310	4446	3913	275	4.00	1.98	0.74	0.39
AT_26	361	18,389	17,959	5936	5376	179	3.82	1.70	0.77	0.42
AT_27	141	13,553	13,157	5424	4675	16	3.62	1.95	0.80	0.43
AT_28	154	13,457	12,923	4300	3927	105	3.96	1.83	0.80	0.42
AT_29	269	17,742	15,904	5489	4437	286	3.09	1.40	0.64	0.33
AT_30	356	37,133	36,514	8291	7266	117	4.01	1.91	0.80	0.42
AT_31	136	16,844	16,366	5021	4521	16	3.19	1.86	0.88	0.47
AT_32	307	23,586	23,323	14,053	12,453	72	3.37	1.92	0.85	0.46
AT_33	329	30,595	29,569	13,949	12,731	104	4.17	2.00	0.80	0.43

Table 1 (continued)

Block name	Number images	Auto-TPs		AutoGCPs		TPs manual	Max. Res. GCP X/Y [m]	Max. Res. GCP Z [m]	RMS GCP X/Y [m]	RMS GCP Z [m]
		Extracted	Retained	Extracted	RETAINED					
AT_34	295	25,694	25,282	15,387	13,817	91	3.81	2.04	0.80	0.46
AT_35	407	38,123	37,500	15,247	13,497	51	3.52	1.81	0.78	0.43
AT_36	312	20,623	20,394	3094	2742	139	3.02	1.77	0.80	0.38

TP statistics across all blocks: RMS TP X/Y = 0.42 pixel

Extracted Auto-TPs/AutoGCPs refers to the number of TPs/GCPs extracted by the data processing routine, *retained* Auto-TPs/AutoGCPs refers to the number of TPs/GCPs active in the last BBA run. *TPs manual* refers to the number of TPs that needed to be added manually

and subsequent elimination of GCPs and/or TPs based on their residuals after running BBA.

On archival aerial images, manual TP digitization turned out to be a fast and relatively convenient technique compared to manual GCP identification and digitization.

To obtain final orientations on the *Emmental* sample block (see Fig. 5), neither manual TPs nor GCPs had to be added to the block. QA work was limited to semi-automatically filtering and de-activating or eliminating TPs and GCPs in the iterative BBA computations. The total amount of human operation time spent to arrive at the final orientations was around 20 min for the whole block. Figure 6 depicts a display of GCP residuals for this sample block. The azimuthal orientation of the residuals appears to be non-systematic.

In general, about 5% of detected TPs and around 25% of detected GCPs were removed during QA to arrive at the final orientations. Depending on the block configuration, the residual threshold for TPs was set to 3 to 4 pixels and the residual threshold for GCPs was set to 15–20 pixels. The required amount of manual work (time) for establishing the final orientations was found to vary significantly between the different blocks. The manual time for QA work largely depended on the number of manual TPs that needed to be added. A number of reasons are found to contribute to incomplete or erroneous point detection. The most important ones are assumed to be input data inconsistencies, land cover, flight block configuration and the parametrization of the alignment process. In some cases, as can be expected, inconsistencies in the input data caused erroneous or no matches for TPs and GCPs. These inconsistencies included, e.g. mismatches between documented and real scan orientation or wrong naming of scan files. The extent of these data input inconsistencies caused problems of local magnitude only, resulting, e.g. in no tie point matches for an affected image. These cases were solved by manually correcting for the base problem. Then, the corrected image was connected to the block again through manual TP measurements. Thanks to a good consistency in data and metadata, the number of such cases was low. In average, less than one image per thousand was affected.

Some of the problems encountered in establishing final orientations were related to land cover. Erroneous matches (blunders) for TPs were, e.g. detected over lake surfaces or surfaces covered by snow or ice. These erroneous matches had to be identified and removed. For the GCP detection these regions were simply masked out from the reference data and presented no problems. For the TP detection, masking out problematic land cover cannot be done directly from, e.g. an existing vector dataset because of the lack of precise orientation data.

A further potential to yield more complete image matching results is believed to lie in optimising parametrization of the alignment process.

Table 1 summarises the statistics for the orientations of all 36 blocks achieved after final QA work. The residuals of GCPs are in the order of 2–3 pixel. A judgement on the quality of orientations based on these GCP residuals may lead though to misinterpretations since we execute no visual control on our automatically extracted GCPs. Furthermore, GCP residuals in our case may have been further reduced by filtering the abundant GCPs without actually improving image orientations. Due to these inherent constraints in the interpretation of GCP residuals, our error analysis therefore focuses on the products. Our principal aim consists in achieving accuracies that allow for generating products that are suitable for the most common applications.

In classical photogrammetric workflows, the quality of orientations is typically assessed by analysing residuals on independent Check Points (CPs). In our case, it may have appeared tempting to simply declare a subset of the abundant amount of GCPs as CPs. This approach was discarded because of the unknown accuracy of the automatically collected reference points. By doing so, a systematic shift amongst automatically collected reference points would, e.g. remain undetected. Alternatively, one might digitise Check Points manually. Since this approach would require the manual work that should be avoided, this approach was discarded as well.

The obtained image orientations allow assessing the accuracies of the initial geo-referencing that was used as input. This information may be used to retrospectively evaluate the plausibility of the defined parameter settings, such as the search radius. Figure 7 displays for each image the planimetric difference in metres between input coordinates and final position of the projection centres. Figure 8a displays the corresponding histogram.

At swisstopo, there exists a large experience in the conduct of orienting AAI using classical photogrammetric workflows. In this context, a classical photogrammetric workflow involves automated fiducial mark detection, automated TP matching but manual GCP digitization from a digital reference source. Due to the heterogeneous nature of AT blocks and the parallel QA conduct of several blocks, comparing the efficiency of the workflow on a per-block base is not an appropriate approach. Efficiency is, therefore, assessed based on the total time spent for the orientation of a country-wide coverage only: in our case, one person, working around 20 h on this project per week, carried out the whole orientation process within 10 weeks. This includes the automatic processing and all manual QA steps for obtaining the final orientations. In consequence, we found that the proposed orientation workflow reduces the human working time massively compared to classical workflows. In our case, we estimate the workflow to be at least five times more efficient in human working time than classical workflows.

3.3 Orthophotos and Mosaics

The geometric accuracy of the final orthophoto mosaic is derived by comparison with the reference orthomosaic. Figure 9 displays the generated country-wide orthophoto mosaic and the geographic distribution of measured differences on the sample grid. Figure 8b shows the histogram of the error distribution. No systematic effects were found in the error distribution. Some of the outliers were identified to be situated in (potentially) unstable alpine terrain. It is likely

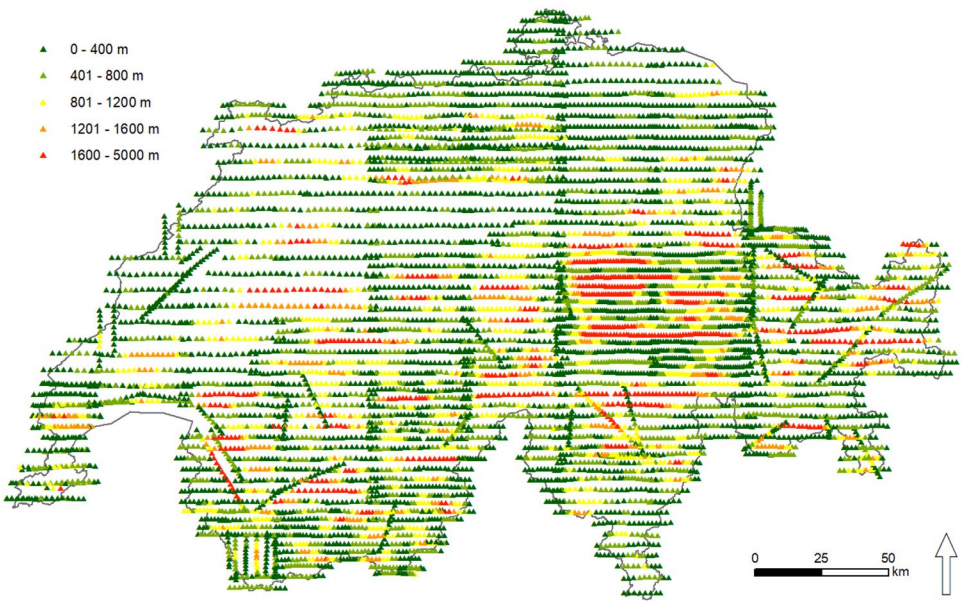

Fig. 7 Planimetric distances in metre between input geo-referencing and final projection centres of images. The mean value amounts to 603.4 m

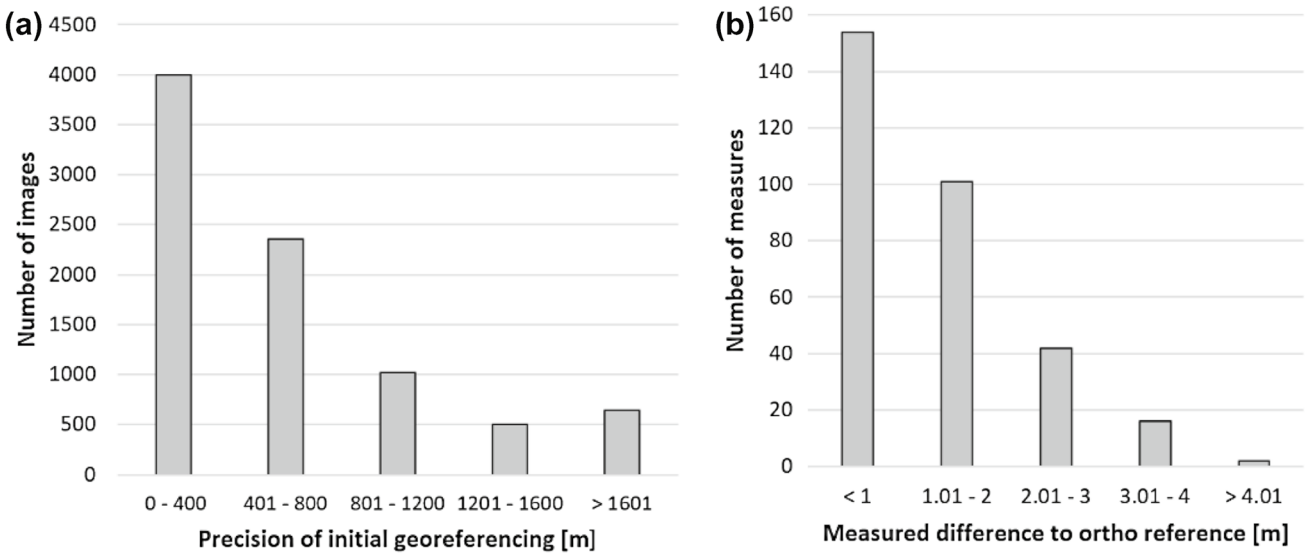

Fig. 8 **a** The histogram evaluates the accuracy of input coarse georeferencing. The mean value is 603.4 m. **b** The histogram depicts the positional accuracy of the derived orthomosaic relative to the orthoreference image. The mean value including the outliers amounts to 1.26 m, the median value amounts to 1.00 m

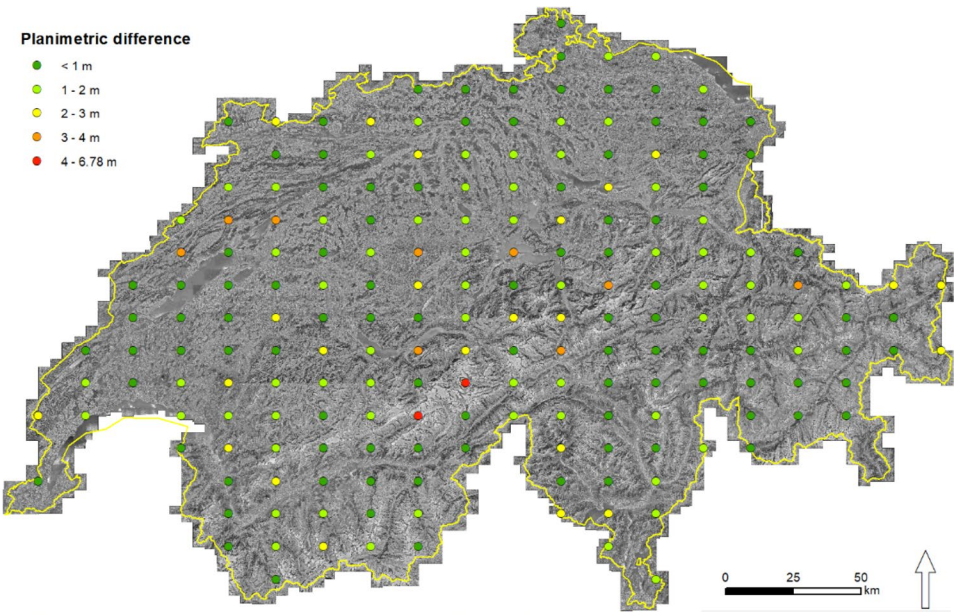

Fig. 9 Results of accuracy assessment from comparing the generated country-wide orthomosaic with the orthoreference. The two red points were identified to be on unstable terrain

that in these cases physical displacement through geomorphological processes between reference and historical air photos has taken place.

Even though the planimetric accuracies obtained for the orthophoto mosaic may lay behind on what may be commonly achieved on local projects (Nebiker et al. 2014; Sevara et al. 2018; Micheletti et al. 2015), the results on the national scale are very satisfying to us. We are convinced that the obtained accuracies allow for most applications of AAI cited in literature. We furthermore believe that the achieved radiometric homogeneity significantly facilitates the visual interpretation of the orthoimagery as well as the use of automated image analysis tools. The evaluated ortho accuracy shows to be in line with the GCP residuals obtained in the orientation process.

3.4 Digital Surface Models

The obtained DSMs showed practically complete coverage. Except for saturated (e.g. snow) or water surfaces, *NoData* values appeared in areas occluded by viewing geometry only. Hillshades of obtained DSMs display fine details and allow

to track topographic changes when comparing to a reference DEM hillshade. The difference of the calculated DSM to the reference DEM is estimated to be better than ± 1 m for around 90% on well-defined surfaces. Well-defined surfaces include, e.g. bare rock, paved surfaces and grassland. Similar accuracies were found in all zones independent from their landscape type. Figure 10 displays examples of the derived DSMs and the orthomosaic.

The results from the DSM extraction are judged to be very satisfying. Since our sample areas for DSM extraction encompass all major land zones, we expect a similar quality for DSMs all over the country-wide data set. The results displayed in Fig. 10 indicate that the extracted DSMs allow for accurate quantification of, e.g. vegetation or glacier volume change on a local to national scale.

4 Discussion

The highlight of the country-wide geo-referencing approach presented here is the complete substitution of manual GCP measurements by an automated process. Automated reference image matching in conjunction with BBA and algorithmic filtering have proven to be efficient substitutes in establishing absolute orientation.

One key factor for successfully employing the proposed workflow to yield precise geo-referencing relates to the quality of input data, corresponding metadata and reference data. Digital image scans should be geometrically precise and radiometrically balanced. Flight geometry needs to assure sufficient lateral and in-flight overlap. Fiducial marks need to be identifiable for successful automated establishment of the interior orientation. Metadata relevant for the processing should be complete and reliable. Accuracy and consistency of reference data directly relate to the accuracy of the absolute image orientation that can be obtained.

These findings lead to the question of transferability of the proposed workflow. Transferability in time looks at the adaptability of the workflow to process other generations of archival aerial imagery over the same area of interest (AOI) revealing different characteristics. Aerial images with differing camera formats, focal lengths, support material (glass plates) etc. are available at swisstopo. Extensive tests, even though not part of this research work, have been carried out on these data. As an outlook to future activities, the results indicate that specific adaptation of processing parameters suffices to successfully process most of the different aerial image types with similar efficiency. The accuracies that can be achieved are a function of the data input quality. An example for another country-wide geo-referencing of aerial images acquired in 1946 (Operation Casey Jones) is given in Heisig et al. (2019). The processing has been performed at swisstopo using the HAP GUI workflow. The input imagery are copies of low quality and no calibration information was available. Despite these unfavourable preconditions, it was possible to produce a country-wide orthomosaic with an absolute accuracy of about 5 m. swisstopo has committed itself to continue processing and publishing further series of archival aerial imagery (swisstopo, 2018).

Transferability in space looks at the possibility of employing the workflow over a different AOI. Our current AOI (Switzerland) covers one of the most complex topographies in Europe. It contains large lake surfaces and is home to the largest glaciers of the Alps. The authors therefore believe that, provided the data input quality is adequate, the workflow is likely to perform well on other AOIs. Adaptations to the processing parameters in function of the input data may be required, though.

However, there is also potential to improve the current workflow. This encompasses the use of further auxiliary data. If available, a mask of unstable terrain for GCP detection might, e.g. be easily integrated. Furthermore, parameter optimization in the alignment process is expected to lead to further reducing manual QA work by providing even more complete TP and GCP patterns. As an example, the matching between image GSD to the orthoreference resolution shall be better controlled to provide optimal results. The HAP and OrthoEngine software is actively developed. Most recent releases contain new functionality such as feature-based matching, enhanced accuracy assessment and automated refinement methods.

One major motivation for the processing of AAI is to ease the access to the information contained for the general public and expert applications alike. Interested users can freely consult the produced year-wise orthophoto mosaics through the national Swiss web-mapping portal at its full resolution (swisstopo 2021a). Other countries' NMCAs chose similar ways to make historic ortho images accessible (Institut national de l'information géographique 2021).In addition, the Swiss confederation has recently adopted and implemented the Open Government Data (OGD) principles for distribution of its national geodata (swisstopo Open Government Data 2021). Image scans and orientation elements, single orthophotos and orthomosaic products can now freely be downloaded or ordered. Users can generate and distribute products from these data with practically no restrictions. Until implementation of OGD principles, a fee-based licence had to be obtained to use the images. The licence primarily was restricted to the use for internal purposes, excluding publication or redistribution of the derived data. OGD-based distribution principles, together with eased technical access, are likely to increase the use of AAI. This may especially hold true for climate change related research activities in alpine environments (Mölg and Bolch 2017; Micheletti et al. 2015).

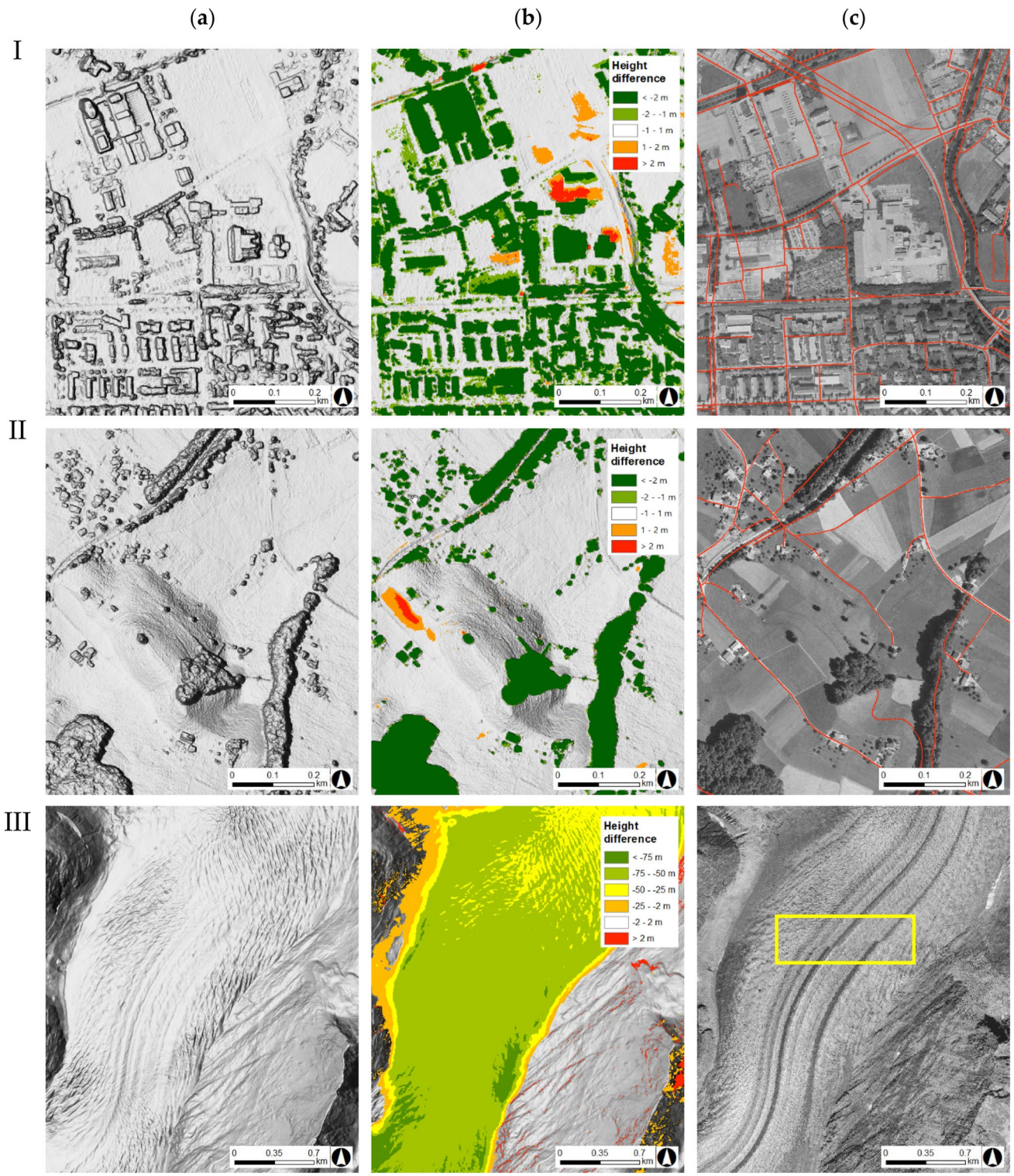

Fig. 10 Examples to illustrate the quality of produced DSM and orthomosaic for (**I**) an urban zone (city of Zürich), (**II**) a rural pre-alpine zone near the lake Thun, (**III**) an alpine zone showing the Aletsch glacier. **a** Shaded relief of the generated DSM. **b** Absolute height difference between the reference DTM and the generated DSM. As the derived DSM is subtracted from a DTM, buildings and vegetation stick out in greenish colours. **c** Orthomosaic overlaid with precise road reference vectors. The planimetric mismatch in (**III**) (yellow box) is due to the use of a recent DTM in the orthorectification process

The centralised fine geo-referencing follows a *once-only* principle. This approach is economically sound because (1) redundancies of multiply orienting images at different customers are avoided and (2) the establishment of an economic production scale at the data provider is fostered. If, however, higher accuracies are required by the user, he/she can further refine the orientations to his/her needs.

Apart from optimising geometry, radiometric processing holds further potential in making information in AAI more accessible. Colorization of panchromatic aerial images, e.g. through means of artificial intelligence is a promising and interesting technique to help colour up our views into the past (Ratajczak et al. 2019).

Acknowledgements Internally, we are grateful to S. Hagmayer for realization of the accuracy assessment and his contributions in the production process, F. Gandor for support with FME and Python, C. Loup for development of PhotoShop macros, E. Raymann for LUBIS management, H. Rusli for general application development, A. Windler for preceding conceptual works and L. O'Sullivan for the English language revision. Externally, we like to thank J.-S. Bouffard and S. Wyseman from PCI Geomatics for reviewing and general support and to Prof. C. Heipke for reviewing and his constructive and helpful comments. For critical suggestions and discussion, we like to thank two anonymous reviewers.

Author Contributions Conceptualization, methodology, and writing—original draft preparation: Holger Heisig; writing—review and editing, and supervision: Jean-Luc Simmen. All the authors have read and agreed to the published version of the manuscript.

Funding This research received no external funding.

Declarations

Conflict of Interest The authors declare no conflict of interest.

References

Bakker M, Lane SN (2017) Archival photogrammetric analysis of river–floodplain systems using Structure from Motion (SfM) methods. Earth Surf Proc Land 42(8):1274–1286

Beyeler A (2010) Arealstatistik der Schweiz-Methodik und aktuelle Ergebnisse. Flächennutzungsmonitoring II. Konzepte–Indikatoren–Statistik. IÖR Schriften 52:111–126

Bożek P, Janus J, Mitka B (2019) Analysis of changes in forest structure using point clouds from historical aerial photographs. Remote Sens 11(19):2259

Cléry I, Pierrot-Deseilligny M, Vallet B (2014) Automatic georeferencing of a heritage of old analog aerial photographs. ISPRS Ann Photogramm Remote Sens Spatial Inf Sci 2(3):33

Cowley DC, Stichelbaut BB (2012) Historic aerial photographic archives for European archaeology. Eur J Archaeol 15(2):217–236

Feurer D, Vinatier F (2018) Joining multi-epoch archival aerial images in a single SfM block allows 3-D change detection with almost exclusively image information. ISPRS J Photogramm Remote Sens 146:495–506

Fischer L, Eisenbeiss H, Kääb A, Huggel C, Haeberli W (2011) Monitoring topographic changes in a periglacial high-mountain face using high-resolution DTMs, Monte Rosa East Face, Italian Alps. Permafrost Periglac Process 22(2):140–152

Fischer M, Huss M, Hölzle M (2015) Surface elevation and mass changes of all Swiss glaciers 1980–2010. Cryosphere 9(2):525–540

Fischler MA, Bolles RC (1981) Random sample consensus: a paradigm for model fitting with applications to image analysis and automated cartography. Commun ACM 24(6):381–395

Ford M (2013) Shoreline changes interpreted from multi-temporal aerial photographs and high resolution satellite images: Wotje Atoll, Marshall Islands. Remote Sens Environ 135:130–140

Ginzler C, Hobi ML (2015) Countrywide stereo-image matching for updating digital surface models in the framework of the Swiss National Forest Inventory. Remote Sens 7(4):4343–4370

Ginzler C, Marty M, Waser LT (2019) Landesweite digitale Vegetationshöhenmodelle aus historischen SW-Stereoluftbildern. Beiträge zur 39. Wissenschaftlich-Technischen Jahrestagung der DGPF e.V.:400–406

Giordano S, Le Bris A, Mallet C (2018) Toward automatic georeferencing of archival aerial photogrammetric surveys. ISPRS Ann Photogr Remote Sens Spat Info Sci 4:105–112

Gomez C, Hayakawa Y, Obanawa H (2015) A study of Japanese landscapes using structure from motion derived DSMs and DEMs based on historical aerial photographs: new opportunities for vegetation monitoring and diachronic geomorphology. Geomorphology 242:11–20

Heipke C (1997) Automation of interior, relative, and absolute orientation. ISPRS J Photogramm Remote Sens 52(1):1–19

Heisig H (2020) Re-Engineering the Past: Countrywide Geo-referencing of Archival Aerial Imagery. Technical Report. A thesis submitted in partial fulfilment of the requirements of Master of Science (Geographical Information Science & Systems) – MSc (GIS). http://unigis.sbg.ac.at/files/Mastertheses/Full/105152.pdf. Accessed 2 Aug 2021

Heisig H, Simmen J-L, Zesiger M (2019) Die Amerikanerbefliegung von 1946 - von selbstentzündlichen Duplikatnegativen zum landesweiten Orthofotomosaik. Geomatik Schweiz(9/2019):268–271

Hirschmuller H (2007) Stereo processing by semiglobal matching and mutual information. IEEE Trans Pattern Anal Mach Intell 30(2):328–341

Institut national de l'information géographique (2016) IGN. Remonter le temps. https://remonterletemps.ign.fr/. Accessed 1 June 2021

Melamed S (2013) Semi-Automated Historical Airphoto Processing. www.pcigeomatics.com/pdf/HAP_WhitePaper.pdf. Accessed 1 June 2021

Mertes JR, Gulley JD, Benn DI, Thompson SS, Nicholson LI (2017) Using structure-from-motion to create glacier DEMs and orthoimagery from historical terrestrial and oblique aerial imagery. Earth Surf Proc Land 42(14):2350–2364

Micheletti N, Lane SN, Chandler JH (2015) Application of archival aerial photogrammetry to quantify climate forcing of alpine landscapes. Photogram Rec 30(150):143–165

Mölg N, Bolch T (2017) Structure-from-motion using historical aerial images to analyse changes in glacier surface elevation. Remote Sens 9(10):1021

Nagarajan S, Schenk T (2016) Feature-based registration of historical aerial images by area minimization. ISPRS J Photogramm Remote Sens 116:15–23

Nebiker S, Lack N, Deuber M (2014) Building change detection from historical aerial photographs using dense image matching and object-based image analysis. Remote Sens 6(9):8310–8336

Nurminen K, Litkey P, Honkavaara E, Vastaranta M, Holopainen M, Lyytikäinen-Saarenmaa P, Kantola T, Lyytikäinen M (2015) Automation aspects for the georeferencing of photogrammetric aerial image archives in forested scenes. Remote Sens 7(2):1565–1593

Persia M, Barca E, Greco R, Marzulli M, Tartarino P (2020) Archival Aerial Images Georeferencing: a Geostatistically-Based Approach for Improving Orthophoto Accuracy with Minimal Number of Ground Control Points. Remote Sens 12(14):2232

Pinto AT, Gonçalves JA, Beja P, Pradinho Honrado J (2019) From archived historical aerial imagery to informative orthophotos: a framework for retrieving the past in long-term socioecological research. Remote Sens 11(11):1388

Ratajczak, R, Crispim-Junior, F C, Faure, E, Fervers, B, Tougne, Le, E., Fervers, B., & Tougne, L (2019) (eds) Toward an Unsupervised Colorization Framework for Historical Land Use Classification. IGARSS 2019 IEEE International Geoscience and Remote Sensing Symposium

Redweik P, Roque D, Marques A, Matildes R, Marques F (2010) Triangulating the past–recovering Portugal's aerial images repository. Photogramm Eng Remote Sens 76(9):1007–1018

Remondino F, Spera MG, Nocerino E, Menna F, Nex F (2014) State of the art in high density image matching. Photogram Rec 29(146):144–166

Sevara C, Verhoeven G, Doneus M, Draganits E (2018) Surfaces from the visual past: recovering high-resolution terrain data from historic aerial imagery for multitemporal landscape analysis. J Archaeol Method Theory 25(2):611–642

Strozzi T, Ambrosi C, Raetzo H (2013) Interpretation of aerial photographs and satellite SAR interferometry for the inventory of landslides. Remote Sens 5(5):2554–2570

Swiss Federal Statistical Office (2013) FSO: Land Use in Switzerland-Results of the Swiss Land Use Statistics, Neuchâtel, Switzerland

swisstopo (2018) Prises de vue terrestres et orthophotos historiques sur map.geo.admin.ch. Geomatik Schweiz 9:274–275

swisstopo (2021a) A journey through time—aerial images. https://www.swisstopo.admin.ch/en/maps-data-online/maps-geodata-online/journey-through-time-images.html. Accessed 1 Jun 2021

swisstopo (2021b) swisstopo Information system for aerial photographs / LUBIS viewer. https://www.swisstopo.admin.ch/en/maps-data-online/maps-geodata-online/lubis.html. Accessed 1 Jun 2021

swisstopo (2021c) swisstopo Swiss national levelling network LN02. https://www.swisstopo.admin.ch/en/knowledge-facts/surveying-geodesy/reference-frames/local/ln02.html. Accessed 28 Jul 2021

swisstopo Open Government Data (2021) OGD. https://www.isb.admin.ch/isb/en/home/themen/e-government/open-government-data-ogd.html. Accessed 1 Jun 2021

swisstopo swissALTI3D (2021) The high precision digital elevation model of Switzerland. https://shop.swisstopo.admin.ch/en/products/height_models/alti3D. Accessed 1 Jun 2021

swisstopo swissimage (2021) The Digital Color Orthophotomosaic of Switzerland. https://www.swisstopo.admin.ch/en/home/products/images/ortho/swissimage.html. Accessed 1 Jun 2021

swisstopo swissTLM3D (2021) The large-scale topographic landscape model of Switzerland. https://shop.swisstopo.admin.ch/en/products/landscape/tlm3D. Accessed 1 Jun 2021

Vargo LJ, Anderson BM, Horgan HJ, Mackintosh AN, Lorrey AM, Thornton M (2017) Using structure from motion photogrammetry to measure past glacier changes from historic aerial photographs. J Glaciol 63(242):1105–1118

Verhoeven G, Sevara C, Karel W, Ressl C, Doneus M, Briese C (2013) Undistorting the past: New techniques for orthorectification of archaeological aerial frame imagery. Good practice in archaeological diagnostics. Springer, Cham, pp 31–67